Composite Structures 328 (2024) 117738

Contents lists available at ScienceDirect

Composite Structures

journal homepage: www.elsevier.com/locate/compstruct

Characterisation of the transverse shear behaviour of binder-stabilised preforms for wind turbine blade manufacturing

P.H. Broberg [a,b,*], F. Shakibapour [b], J. Jakobsen [b], E. Lindgaard [a,b], B.L.V. Bak [a,b]

[a] CraCS Research Group (cracs.aau.dk), Aalborg University, Fibigerstræde 16, DK-9220, Aalborg East, Denmark
[b] Department of Materials and Production, Aalborg University, Fibigerstræde 16, DK-9220, Aalborg East, Denmark

ARTICLE INFO

Dataset link: /10.17632/9m78sg3zwn.1

Keywords:
Fabrics/textiles
Binder-stabilised preforms
Transverse shear
Cyclic loading
Composite manufacturing

ABSTRACT

Binder-stabilised preforms are being used increasingly in the production of large composite structures, such as wind turbine blades, to increase the throughput. The transverse shear behaviour of the preform is one of the driving factors in the development of wrinkling during manufacturing but has not previously been characterised in the literature. In this paper, the combined intra- and inter-ply deformations during transverse shearing of a binder-stabilised preforms for wind turbine blade manufacturing are characterised by a new test methodology. The results from two experimental campaigns are presented. In the first campaign, preform specimens are subjected to monotonic loading to a nominal transverse shear angle of 18.0° with three different deformation rates. The results show an increase in maximum load levels with greater deformation rates. In the second campaign, preform specimens are subjected to deformation-controlled cyclic loading with two different deformation amplitudes corresponding to a nominal transverse shear angle of 1.5° and 12.2°, respectively. During cyclic loading, permanent deformation is observed in all preform specimens and the maximum load at the 19th cycle is reduced to 48% of the maximum load at the first cycle for the tests with deformation amplitudes of 12.2°. The data generated in this study is freely available at https://doi.org/10.17632/9m78sg3zwn.1.

1. Introduction

To reduce the production cost and increase the throughput of composite structures, the simultaneous forming of multi-layered stacks of fabrics is being used increasingly. This is both done in hot-drape forming of aerospace structures [1], and resin transfer moulding of automotive parts [2]. Lately, stacks of dry non-crimp fabrics (NCFs) with a binder between each layer (binder-stabilised preforms) are also getting interest in the production of wind turbine blades [3,4]. The focus of this work is on binder-stabilised preforms used in the production of wind turbine blades.

Uncured composite materials are prone to defects due to a lot of uncertainties involved in manufacturing [5]. During forming of composite parts, some of the most significant defects arising are fibre waviness or out-of-plane wrinkling [6]. These wrinkles can lead to a severe knock-down in the strength of the finished solidified composite part [7]. For wind turbine blades, the knock-down in strength has been investigated in [8–10], with an observed knock-down of 66% for some wrinkle configurations [10]. Numerous studies have investigated the mechanisms leading to wrinkling in composite forming. Considering a single ply, one of the driving mechanisms for wrinkling is the inability of the ply to conform to a double-curved mould through in-plane shearing [11–13]. However, when multiple plies are formed together, the properties of the interface between the individual plies greatly influence the wrinkle creation [14–18]. Specifically, the risk of fibre wrinkling increases when the plies are not capable of moving relative to each other. This risk may increase for plies of similar orientation due to an increase in friction [19]. In composite manufacturing with binder-stabilised preforms, the polymeric binder serves the purpose of stabilising the preform to avoid wrinkling during handling of the uncured preform and to significantly reduce the layup time in the main mould [20,21]. On the other hand, the binder may also impede inter-ply movement, which may lead to wrinkles during forming. These wrinkles are, typically, located at single or double curvature geometric transitions [22]. An example of such a transition is a ramp, illustrated in Fig. 1, which is common at core material transitions in wind turbine blades. To achieve wrinkle-free forming of preforms, a trade-off between stability and formability of the preform is sought.

* Corresponding author at: Department of Materials and Production, Aalborg University, Fibigerstræde 16, DK-9220, Aalborg East, Denmark.
E-mail addresses: phb@mp.aau.dk (P.H. Broberg), fahimeh@mp.aau.dk (F. Shakibapour), joj@mp.aau.dk (J. Jakobsen), elo@mp.aau.dk (E. Lindgaard), brianbak@mp.aau.dk (B.L.V. Bak).

https://doi.org/10.1016/j.compstruct.2023.117738
Received 7 July 2023; Received in revised form 2 October 2023; Accepted 20 November 2023
Available online 22 November 2023

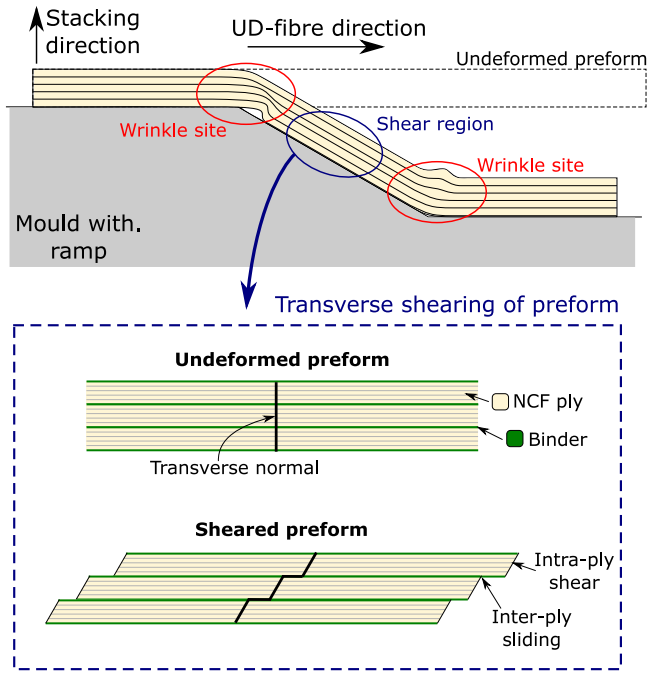

Fig. 1. Illustration of the forming of a binder-stabilised preform over a ramp. At the transition edges, wrinkles may appear if the preform does not undergo transverse shearing (top). The preform shear is a combination of intra-ply and inter-ply deformations (bottom).

Numerical simulation models may be used to help assess the formability of multi-layered preforms and defect generation during forming [17,22,23]. These models require accurate characterisation of relevant deformation modes, which includes the transverse shear behaviour for binder-stabilised preforms. The two overall mechanisms that govern transverse shearing of the preform are intra-ply shearing and inter-ply sliding. The inter-ply sliding is the relative movement of the NCFs with respect to each other, while the intra-ply shearing occurs when the fibres in the NCF slide relative to each other. Notice that, intra-ply shearing in this context refers to the out-of-plane transverse shearing of the NCF and not the in-plane shearing. Several experimental setups for characterising the inter-ply behaviour of fabrics used in the manufacturing of composite structures are described in the literature. They can, generally, be divided into two overall categories: sled-type tests and pull-through/pull-out tests. For the sled-type tests, the normal load is applied by weights [24–26] whereas, pull-through/pull-out tests apply normal loads by clamps [27–33]. These setups have both been used to characterise the friction between dry fabrics (woven or NCF) [24,26,30], non-consolidated fabrics with binder dispersed on top [25], and prepreg material systems [27–29,32,33]. Recently, a custom-built setup has been used to study the friction between carbon NCFs under vacuum to emulate double-diaphragm forming processing conditions [34].

The intra-ply shear of thermoplastic UD melts has been characterised by [35] using a torsional test rig. A custom-made shear rig was designed to characterise the intra-ply shearing on yarn level in [36]. More recently, the intra-ply shear of UD-tapes has been characterised using Timoshenko beam theory on bent fabrics in a dynamic mechanical analysis (DMA) [37]. All current methods of measuring the intra-ply shearing of fabrics are used on UD composite materials. To the author's knowledge, no general applicable methodology for characterising the through-thickness intra-ply shearing of NCF and other fabrics has been described in the literature. To characterise the intra-ply transverse shear stiffness of thick 3D woven (interlock) fabrics a custom-built transverse shear fixture was made in [38]. Variations of this setup are described in [39] and, more recently, in [40]. A similar test fixture is used to characterise the shear properties of sandwich core material in ASTM C 273 [41].

During handling of the binder-stabilised preform and placement in the main casting mould, the preform may be subjected to repeated loading. During repeated loading, fabric materials often show strong hysteretic behaviour. This has been observed in [42,43] where the static coefficient of friction was shown to decrease with repeated loading. The reason for this was argued in [42] to be due to abrasion and reorganisation of the fibres inside the yarns. However, both studies were carried out on woven fabrics that may be more unstable than NCFs and, thus, more susceptible to fibre reorganisation.

Currently, the state-of-the-art for characterising binder-stabilised preforms consists of inter-ply friction tests. As this test does not take into account the intra-ply shearing of the NCFs, the transverse shear behaviour of binder-stabilised preforms remains unclear. Measuring the intra-ply shear characteristics on a single NCF is challenging because it is difficult to fix the top and bottom of the NCFs. Furthermore, current process models for assessing the formability of preforms in wind turbine blade manufacturing consider the combined effect of inter-ply sliding and intra-ply shearing when modelling transverse shearing [22].

The aim of this study is to characterise the transverse shear behaviour of dry binder-stabilised preforms for wind turbine blade manufacturing (consisting of mainly UD-NCFs) during both monotonic and cyclic loading. To achieve this, a new experimental methodology for experimental characterisation and data processing of the transverse shear behaviour of thick preforms is presented. The main novelty associated with the work presented in this paper is the characterisation of the transverse shear behaviour of a dry binder-stabilised preform material system. The results of such a characterisation are important for studying preform formability and are, to the authors' knowledge, yet to be reported in the literature. The preform used in this study is representative of what is used in wind turbine blade manufacturing. The rest of the paper is structured as follows: in Section 2 the test fixture is presented with a description of the preform material tested. The results are presented in Section 3 and discussed in Section 4. Finally, the paper is concluded in Section 5.

2. Material and methods

2.1. Preform shear test fixture

To carry out transverse shear tests of dry binder-stabilised preforms, a test fixture is designed that can be mounted in a standard tensile test machine. The fixture consists of two L-shaped aluminium blocks with a widened slot on one surface of each block such that it can be mounted in the grips of the test machine with a threaded rod. The slot allows for adjusting the threaded rod to make the shear load apply to the centre line of specimens with varying thickness. One of the L-shaped blocks is fixed during testing, while the other is moved by the cross-head of the test machine. Each block consists of a horizontal and vertical part that are supported by a bracket to prevent significant deflection during loading of the specimen. Two disposable aluminium plates are screwed to the blocks, and the preform specimen is glued in between the aluminium plates. To measure displacement during the test, a Crack Opening Displacement (COD) gauge extensometer is mounted between two COD gauge plates. A schematic of the test fixture is shown in Fig. 2. The fixture is installed in an Instron ElectroPuls *E10000* test machine as shown in Fig. 3. The block, which is clamped to the lower part of the machine, is the fixed block, whereas the moving block is clamped to the upper part of the machine. Both the fixed and moving blocks are gripped in a set of vee wedge jaws with a fully threaded rod such that the shear load applies to the centre line of the preform test specimens.

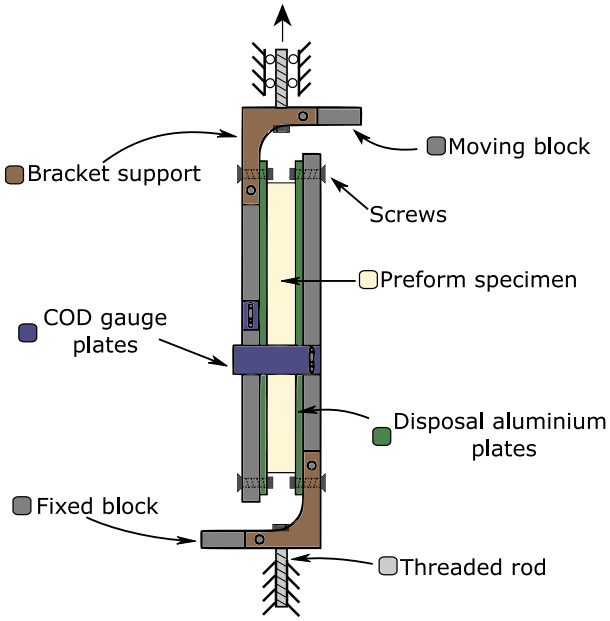

Fig. 2. Test fixture configuration.

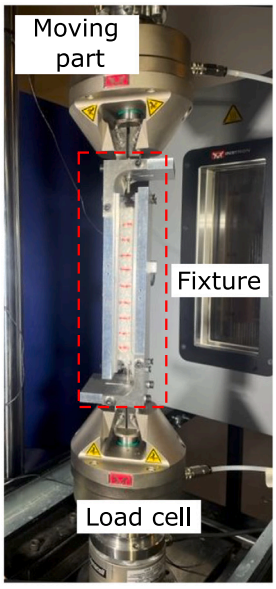

Fig. 3. The test fixture mounted in the test machine.

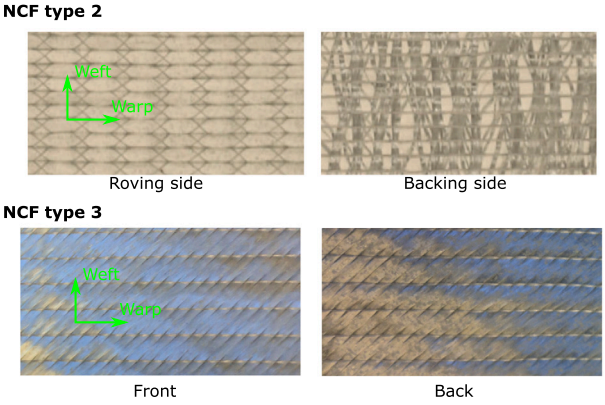

Fig. 4. Non-crimp fabrics (NCFs) used for the preforms specimens. NCF type 1 is uni-directional and has an architecture similar to NCF type 2.

2.2. Testing procedure

A 10 kN load cell is used for the test. The load cell and the COD are zeroed before running each test. All tests are carried out at room temperature. Two different test campaigns are carried out: a monotonic test campaign and a cyclic test campaign. In the monotonic tests, the specimens undergo 6.0 mm displacement at three different speeds of the cross-head: 2 mm/min, 20 mm/min and 60 mm/min, respectively. A displacement of 6.0 mm corresponds to an average shear angle of 18.0° for the specimens tested. The target shear angle was chosen based on the initiation of interface failure, see Fig. 9. Five repeats with pristine specimens are carried out for each deformation rate. The displacement and force are logged during the experiment.

Cyclic testing is carried out, as the preform is loaded repeatedly during transport, handling and placement when manufacturing wind turbine blades. Depending on the level of the loading, this may need to be accounted for in the process modelling. The cyclic tests are carried out with a speed of the cross-head of 20 mm/min with two different displacement amplitudes for the loading–unloading loops. For the first case, each sample is cycled 50 times with a triangular cyclic function for the displacement with a mean equal to 0.0 mm and an amplitude equal to 0.5 mm. A displacement of 0.5 mm corresponds to an average shear angle of 1.5° for the tested specimens (small displacement amplitudes). For the second case, each sample undergo 20 cycles with a triangular cyclic function for the displacement with a mean equal to 0.0 mm and an amplitude equal to 4.0 mm. A displacement of 4.0 mm corresponds to an average shear angle of 12.2° for the tested specimens (large displacement amplitudes). For each case, 5 repeats are carried out with pristine specimens. The two displacement amplitudes are chosen to investigate either side of the transition point between the shear and the interface degradation zone for the monotonic tests, see Fig. 9.

A monochrome 5MP *FLIR Blackfly S* camera with a 25 mm *Fujinon* lens that is synchronised with the displacement is used to acquire images of the side of the specimen at a rate of 7 Hz for the monotonic tests and 1 Hz for the cyclic tests.

2.3. Material and sample fabrication

The results from characterising a single type of preform specimen is presented in this paper. The tested preform consists of three types of glass fibre NCFs that are described in the following. NCF type 1 has an area weight of 712 g/m^2. It consists of 92 wt% H-glass fibres oriented at 0 degrees. There are 8 wt% E-glass backing fibres oriented at ±80 degrees. The fibre angles are given relative to the warp direction of the fabric; see Fig. 4. The stitch is a combined tricot-chain of polyester thread. The thickness of NCF type 1 is approximately 0.5 mm. NCF type 2 has an area weight of 1380 g/m^2. It consists of 96 wt% H-glass fibres oriented at 0 degrees. There are 4 wt% E-glass backing fibres oriented at ±80 degrees. The fibre angles are given relative to the warp direction of the fabric: see Fig. 4. The stitch is a combined tricot-chain stitch of polyester thread. The thickness of NCF type 2 is approximately 1.0 mm. NCF type 3 has an area weight of 806 g/m^2. It consists of H-glass fibres oriented at ±45 degrees. The fibre angles are given relative to the warp direction of the fabric; see Fig. 4. The stitch is a chain stitch of polyester thread. The thickness of NCF type 3 is approximately 1.0 mm.

The preform specimens are made of 21 layers of glass non-crimp fabric. The layup of the preform with the three types of NCF is listed in Table 1 and sketched in Fig. 5. The preform is consolidated using a soluble polyester binder that are dispersed as powder on the roving side of the fabric. The binder is activated by consolidating the preform at elevated temperatures. The binder primarily bonds the backing fibres of one NCF to the rovings of the adjacent NCF. The total thickness of the preform specimens is 18.5 mm.

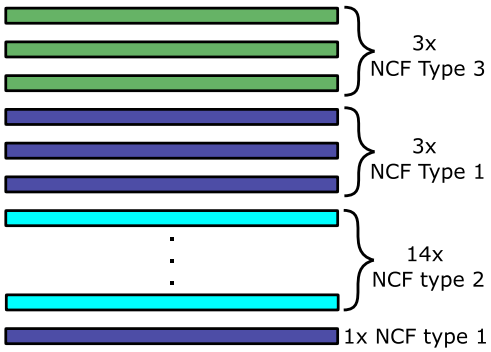

Fig. 5. Sketch of the layup of the preform specimens.

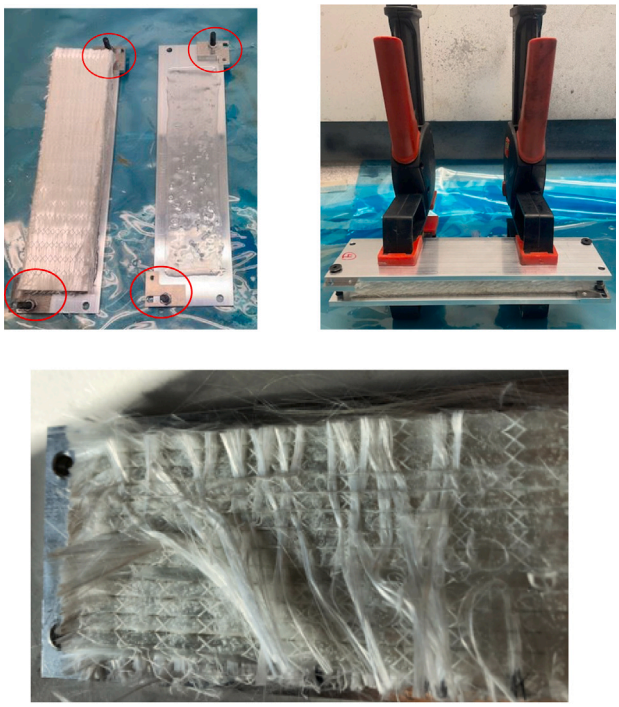

Fig. 6. Alignment of the specimens on the disposable aluminium plates. The four alignment plates are highlighted with the red circles (top left). A light pressure is added to the specimens during curing of the glue (top right). The glue is penetrating layer 1, which is observed by the backing material of the adjacent plies sticking to the plies (bottom).

Table 1
Layup of the preform specimens.

Layer Nr.	1	2–15	16–18	19–21
NCF type	Type 1	Type 2	Type 1	Type 3

The preform specimens are glued to the aluminium plates with *Permalock EP-708* 2-component epoxy glue at room temperature. The contribution of the thickness of the glue to the total thickness of the specimen is assumed negligible. During specimen preparation, it is important that the preform is aligned with the load direction. To ensure that, four alignment plates are mounted on the disposable plates to position the preform samples in the middle of the plates, as shown in Fig. 6. Two clamps are used to apply a small amount of pressure during the curing of the glue while avoiding the glue to penetrate into the preform, see Fig. 6. After curing, the penetration of the glue was investigated by carefully removing one fabric layer at a time. It was observed that the glue penetrates layer 1 (see Fig. 6). No penetration of the glue was observed in the other layers. With a thickness of approximately 0.5 mm of layer 1, the influence of the glue penetration on the transverse shear behaviour is negligible. As a final preparation step, the alignment plates are removed from the disposable plates and the prepared sample may be installed in the test fixture and tested.

The preform specimen, glued in between the two disposable plates, has the size of 200 mm × 50 mm × 18.5 mm (Length × Width × Thickness).

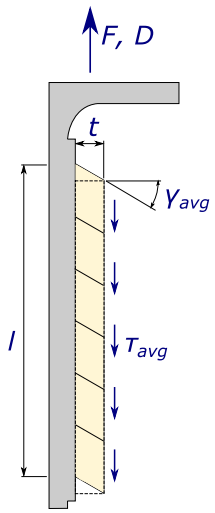

Fig. 7. Stresses transferred to the preform specimen during loading. It is assumed that the shear stresses are distributed evenly over the cross-sectional area and that the specimen is shearing evenly over the entire thickness.

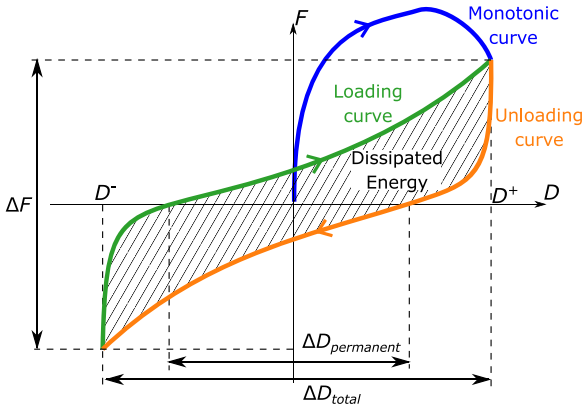

Fig. 8. The hysteresis curve from the cyclic tests consists of a loading curve and the subsequent unloading curve. The first part of the curve, from the start of loading until the first reversal of load, is referred to as the monotonic curve. The dissipated energy for a cycle is calculated as the area inside the hysteresis curve. Definition of displacement ranges and load ranges are given in the figure.

2.4. Data processing

The test fixture enforces a simple shear deformation on the preform specimen [44]. It is assumed that the test specimen deforms in simple shear and that the only stresses transferred to the preform specimen are shear stresses, as shown in Fig. 7. From the load cell and clip gauge, respectively, load (F) and displacement (D) data are available. Based on these, the average shear stress and average shear angle for the preform specimen are calculated by,

$$\gamma_{avg} = \tan^{-1}\left(\frac{D}{t}\right), \quad \tau_{avg} = \frac{F}{lw} \tag{1}$$

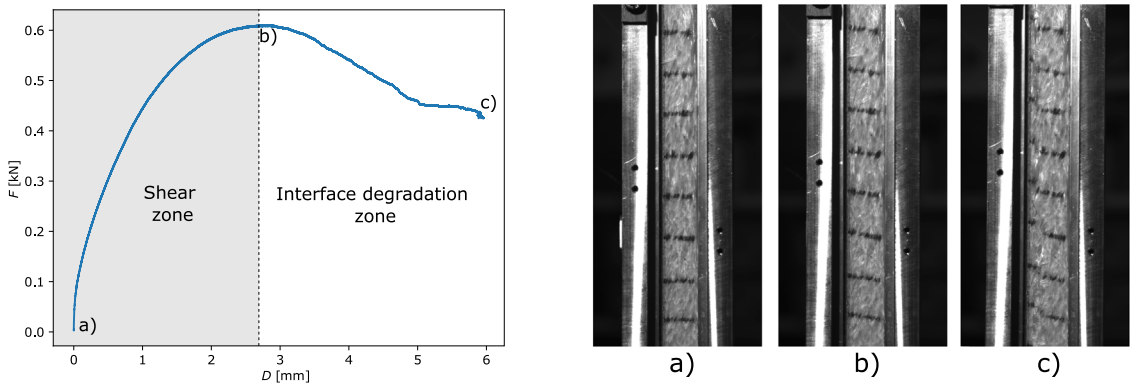

Fig. 9. Load–displacement curve for one of the monotonic loading tests of the preform with a displacement rate of 2 mm/min (left). Images of the specimen during loading (right): (a) undeformed specimen, (b) sheared specimen at the maximum load and (c) specimen at the end with damages in the interface.

where D is the displacement of the fixture, F is the cross-head load, t is the specimen thickness, l is the length of the specimen, and w is the width of the specimen. In the monotonic tests, D is based on the COD displacement, while the cross-head displacement is used in the cyclic tests as the COD offsets the measured displacement at a high number of cycles.

For the cyclic tests, the hysteresis curve is considered, as shown in Fig. 8. The deformation curve from the start of the loading (prescribed displacement) until the first reversal of load (at D^+) is referred to as the monotonic curve. The unloading curve that follows the monotonic curve (from D^+ to D^-) is, together with the monotonic curve, referred to as cycle 0 (Fig. 13). The first cycle starts from D^-, then loaded to D^+, and then unloaded to D^- again. After that, every cycle consists of loading and then unloading in that order. This means that cycle 19 is the last cycle for the test with a displacement amplitude of 4.0 mm, while cycle 49 is the last cycle for the test with a displacement amplitude of 0.5 mm.

For each cycle, the energy dissipated is computed as the area inside the hysteresis curve (Fig. 8). The permanent deformation, $\Delta D_{permanent}$, is defined as the deformation range between the hysteresis curve at $F = 0$. From the permanent deformation range and the total deformation range, ΔD_{total}, the elastic deformation range is defined as,

$$\Delta D_{elastic} = \Delta D_{total} - \Delta D_{permanent} \tag{2}$$

With this definition, the elastic deformation is a measure of the deformation that are recovered during one cycle. The amount of softening at cycle i is determined by the ratio,

$$R_{softening,i} = \frac{\Delta F_i}{\Delta F_0} \tag{3}$$

where ΔF_i is the load range at cycle i as shown in Fig. 8, and ΔF_0 is the load range at the zeroth cycle.

3. Results

The raw data from all test cases are freely available at https://doi.org/10.17632/9m78sg3zwn.1. The resulting load–displacement curve for one of the monotonic tests with a deformation rate of 2 mm/min is shown in Fig. 9. This result is typical and representative of what is observed in all the monotonic tests. The results from the monotonic test are divided into two zones: the shear zone and the interface degradation zone. The shear zone is characterised by increasing shear stresses for increasing shear angles and visible uniform shearing on the test specimens, see Fig. 9. The interface degradation zone is characterised by a decrease in the load level for increasing deformations and visible non-uniform shearing across the specimen. This non-continuity in the specimens may be due to either damage in the interface or the NCF (such as breakage of stitching or wrinkling). Post-mortem investigations on the specimens have been carried out by carefully separating the NCFs and observing the fibre architecture. In the damaged interfaces the binder interface was broken and no longer holding the adjacent NCFs together, making the NCFs easy to separate, while the nondamaged interfaces were more difficult to separate due to the intact binder interface. An image of the NCF in a damaged and nondamaged interface is shown in Fig. 10. In the damaged interface some of the fibres have been 'pulled' between the stitches, which causes fibre waviness in the rovings. The stitching remains intact in both the damaged and nondamaged interface.

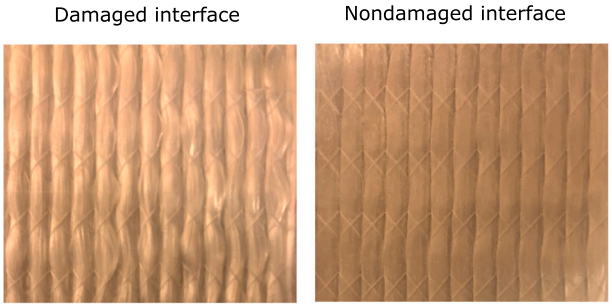

Fig. 10. Images of the post-mortem inspection of the deformed specimens. Fibre waviness is observed in the damaged interface.

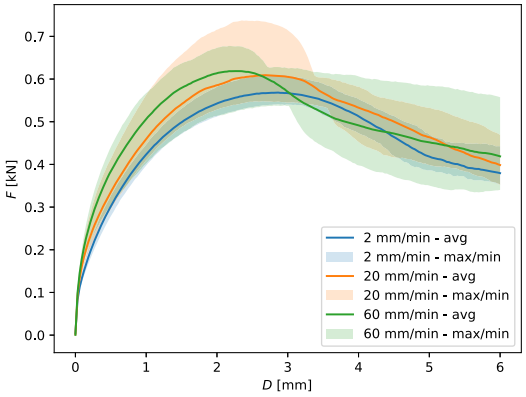

Fig. 11. Average load–displacement curves for the shear testing at three deformation rates. The shaded area indicates max and min bands.

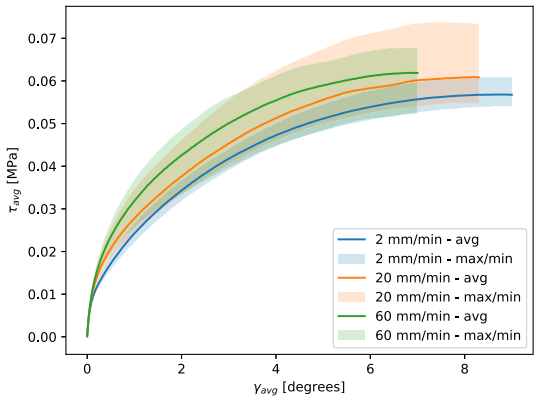

Fig. 12. Comparison of the τ_{avg}-γ_{avg} curves for different deformation rates. The results are not truncated at the same shear angle, due to the degradation point (point b in Fig. 9) being different for different deformation rates.

Table 2
List of permanent and elastic deformation (as defined in Section 2.4) of the average hysteresis loops. The ratio listed in this table is the ratio of permanent to total deformation.

Test	$\Delta D_{permanent}$	$\Delta D_{elastic}$	$\frac{\Delta D_{permanent}}{\Delta D_{total}}$
1st cycle			
0.5 mm	0.493 mm	0.507 mm	0.493
4.0 mm	3.80 mm	4.20 mm	0.475
4th cycle			
0.5 mm	0.516 mm	0.484 mm	0.516
4.0 mm	4.22 mm	3.78 mm	0.528
19th cycle			
0.5 mm	0.543 mm	0.457 mm	0.543
4.0 mm	4.54 mm	3.46 mm	0.568
49th cycle			
0.5 mm	0.564 mm	0.436 mm	0.564
4.0 mm	–	–	–

3.1. Monotonic loading with different deformation rates

The resulting load–displacement curves from the monotonic test with the three different deformation rates are shown in Fig. 11. As the deformation rate increases, the load levels in the shear zone, generally, increase. The variability in the results (indicated by the width of the max–min bands) increases with increasing deformation rates. The τ_{avg}-γ_{avg} curves for the preform specimens are shown in Fig. 12. The curves are only shown in the shear zone, cf. Fig. 9, as the assumption of uniform shear across the thickness of the specimen is not valid in the interface degradation zone defined in Fig. 9. The maximum relative difference between the average τ_{avg}-γ_{avg} curves for the 2 mm/min and 20 mm/min deformation rates is 26.70% (at low shear angles), while the minimum relative difference is 8.19% (close to the maximum load). The average relative difference is 11.81%. The maximum relative difference between the average τ_{avg}-γ_{avg} curves for the 2 mm/min and 60 mm/min deformation rates is 44.94% (at low shear angles), while the minimum relative difference is 11.61% (close to the maximum load). The average relative difference is 23.40%. The shear zone, cf. Fig. 9, based on the averaged curves is smaller for greater deformation rates. The start of the interface degradation zone, for the specimens tested, is 9.0° at 2 mm/min, 8.3° at 20 mm/min, and 7.0° at 60 mm/min, as indicated by the maximum load in Fig. 11. The transverse shear stiffnesses are similar at intermediate shear angles, however, at low shear angles the stiffness increases at larger deformation rates.

3.2. Cyclic loading

Test data from a cyclic test with a displacement amplitude of 0.5 mm and a test with a displacement amplitude of 4.0 mm are shown in Fig. 13. The results from the two tests are representative of the other tests. The images of the specimen in Fig. 13 are from the test with a displacement of 4.0 mm. The deformation of the preform specimens is too small to be visible on the images of the specimens tested with the displacement amplitude of 0.5 mm. The displacement of 4.0 mm is in the interface degradation zone (cf. Fig. 9), which indicates that some slip in the interface is expected already at the zeroth cycle. However, the deformation of the specimen at the zeroth cycle in Fig. 13 is mostly uniform, which means that the interface degradation at the zeroth cycle is expected to be minimal. During testing the deformation changes from being mostly uniform to concentrated at a single interface for the last cycle (19th cycle). This is observed both at 4.0 mm and −4.0 mm displacement.

The softening factor as a function of cycle number is shown in Fig. 14. The averaged softening factor in the specimens tested with a displacement amplitude of 0.5 mm is 0.84 at the 19th cycle, while it is 0.48 for the specimens tested at 4.0 mm. This difference in softening for the 0.5 and 4.0 mm displacement case is also evident in Fig. 13. The energy dissipated per cycle of the cyclic experiments is shown in Fig. 15. The shape of the curves for the dissipated energy is similar for tests with the same displacement amplitude, but there is some variation in the amount of energy dissipated as demonstrated by Fig. 15. The averaged hysteresis curves at the 19th cycle, for both the 0.5 mm and 4.0 mm case, is shown in Fig. 16. Permanent deformation is observed in both cases. The permanent deformation, elastic deformation, and the ratio of permanent to total deformation are listed in Table 2 at different cycles. The ratio of permanent to total deformation is increasing with increasing number of cycles. Post-mortem inspection of the specimens tested in cyclic deformation showed the same tendencies as for the specimens tested in monotonic loading, ie. no damage to the stitching, but some buckling of the UD-roving, see Fig. 10.

The shape of the monotonic curves is compared with the cyclic loading and unloading curves at the 19th cycle (cf. Fig. 8) in the following to study the symmetry of the hysteresis curve, and the difference between the monotonic and cyclic loading curves. The unloading curve is rotated 180° to compare it with the loading curve. Both the loading and the unloading curves are translated to start at (0,0) to compare them with the monotonic curve. The results of the comparison for both the 0.5 mm and 4.0 mm cases are shown in Fig. 17. There is a good agreement between the monotonic curve, and the cyclic loading and unloading curve for the 0.5 mm case, while the difference between the monotonic and cyclic curves for the 4.0 mm case is substantial.

4. Discussion

In the previous section, the results from characterising the transverse shear behaviour of a binder-stabilised preform subjected to monotonic and cyclic loading have been presented. To aid the discussion, the main deformation modes of the individual NCFs in the preform are sketched in Fig. 18. It is out of the scope of this paper to present a model for representing the transverse shear behaviour of the preforms, however, some considerations and observations will be incluæded in this discussion to support future modelling of preforms. The preform characterised in this work primarily consists of quasi uni-directional non-crimp fabrics (UD-NCFs). The term ‘quasi’ indicates that the UD-NCFs have been stabilised with a backing layer. During transverse shear deformation of the preform, the NCFs may deform either due to intra-ply shearing or inter-ply sliding. The contribution of the binder shearing is limited as the thickness of the binder interface is negligible. The mechanisms that may cause intra-ply shearing are: sliding of fibres in the UD-roving, sliding between UD-rovings and backing, and instabilities of fibres, as outlined in Fig. 18.

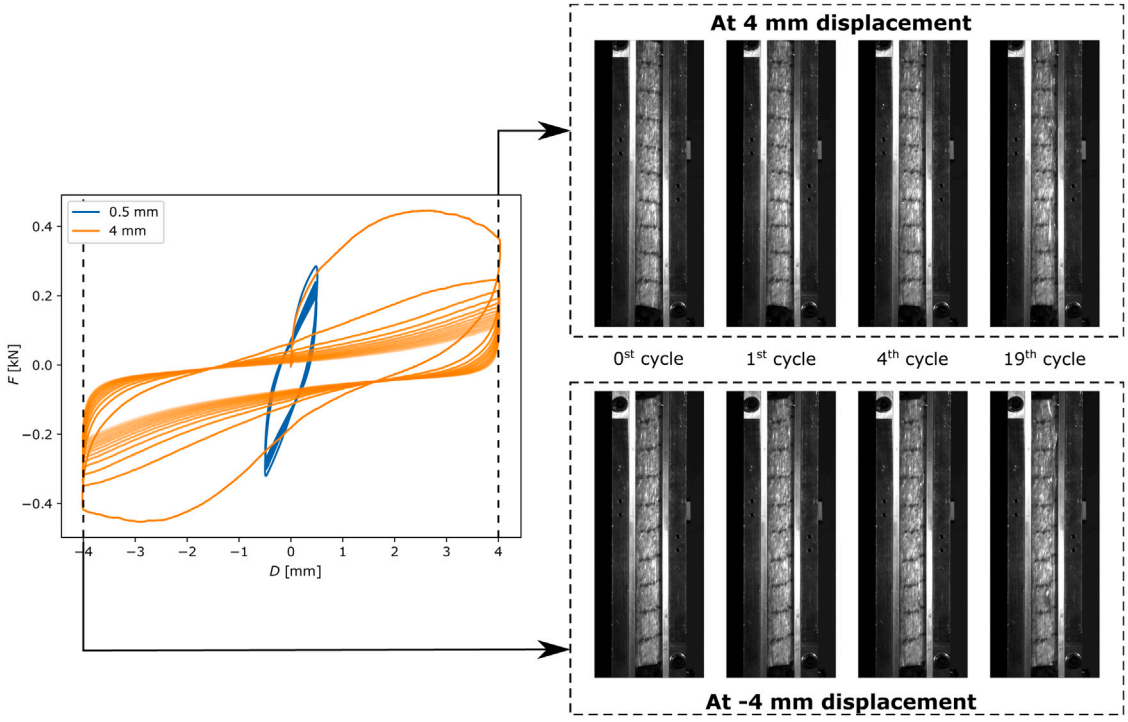

Fig. 13. Load–displacement curve from one of the cyclic tests using a displacement amplitude of 0.5 mm and a cyclic test using a displacement amplitude of 4.0 mm (left). Images of the deformed specimen at 4 mm and −4 mm displacement for the 0th, 1st, 4th and 19th cycle, respectively (right).

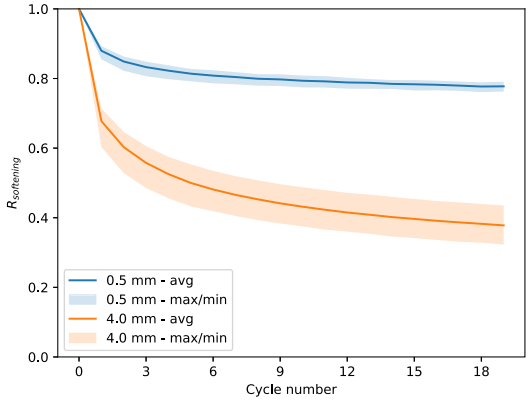

Fig. 14. Softening factor as a function of cycle number for the cyclic tests with an amplitude of 0.5 mm (blue curve) and 4.0 mm (orange curve).

The load–displacement curves from the monotonic tests are divided into two zones: the shear zone and the interface degradation zone (Fig. 9). In the shear zone (before the maximum load level is achieved), the preform specimens undergo uniform shearing across the thickness, while non-uniform shearing is observed in the interface degradation zone. From the post-mortem investigations of the preform specimens, it was observed that the binder interface was broken and no longer holding the adjacent NCFs together. Furthermore, the rovings were pulled-out at the non-uniform interfaces. Similar damage has been observed in literature with waviness and roving pull-out in ply-ply interfaces observed in [24], and damage to binder yarns of 3D fabrics (interlock) for large shear angles observed in [39]. For the interfaces that were shearing uniformly, no loss of adhesiveness of the binder and buckling of rovings were observed when separating the layers post mortem. In this case, the main deformation may occur by sliding between the UD rovings and backing as previous literature suggests that the inter-ply friction is lower for rovings oriented perpendicular to each other than for parallel rovings [19,34]. The buckling of the rovings observed in the non-uniform interfaces is not desired during manufacturing as it could cause a knock-down in the strength of the composite part. This means that the preform ideally should remain in the shear zone during manufacturing.

The average load level in the shear zone is increased with increasing deformation rate as shown in Fig. 12. Similar observations have been made on prepreg material systems [29,31,33], which indicates that the polymeric binder may contribute to the viscous behaviour of the preform. Furthermore, it is observed that the shear zone gets smaller with increasing deformation rates. This may be due to the increase in load levels accelerating the onset of interface damage.

From the images of the specimen during large displacement cyclic loading (cf. Fig. 13), it is observed that the shear deformation initially is uniform across the thickness of the preform while later in the test being concentrated at a single interface. No damage to the stitching and only minor buckling to the rovings in the NCFs are observed post-mortem. This indicates that the transition from uniform to concentrated shearing primarily is due to damage development in the binder interface. Softening of the shear response was observed during cyclic loading. This softening was more pronounced for the large displacement amplitude cyclic tests. The softening observed for the small displacement cyclic tests may be due to abrasion or fibre straightening [43], which decreases the friction between fibres in a roving or between the backing and UD-rovings. The energy dissipated during each cycle is shaped similarly to the softening response. This is due to the shape of the hysteresis curve not changing much during repeated loading. The dissipated energy may result in heat generation which can affect the properties and behaviour of the binder material. However, this is not considered a problem, because of the relatively low loads involved in the forming of a preform.

Both permanent and elastic deformation are observed in the tests (see Table 2). Fibre sliding may lead to permanent deformation in the preform, while elastic deformation may arise due to fibre instabilities, pulling of stitching and elastic deformation of the binder. Interestingly, the ratio between the elastic and permanent deformation is similar

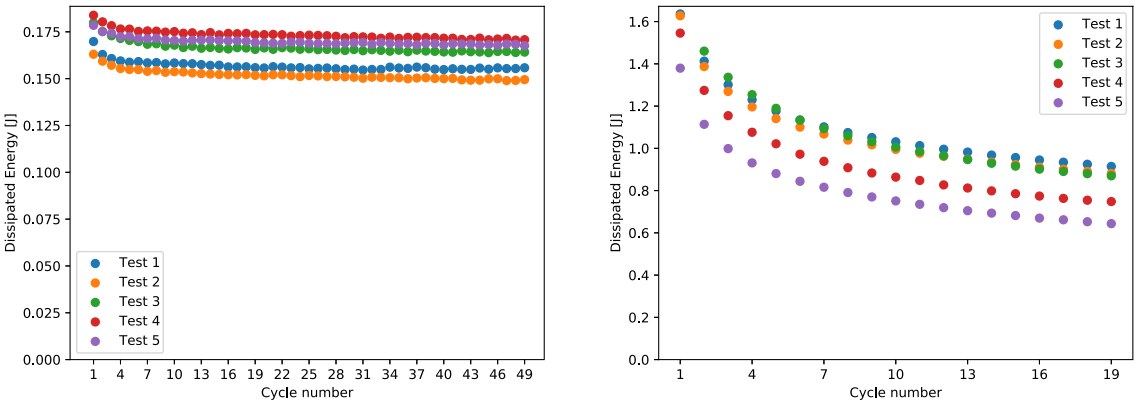

Fig. 15. Energy dissipated per cycle for the test with an amplitude of 0.5 mm (left) and 4.0 mm (right).

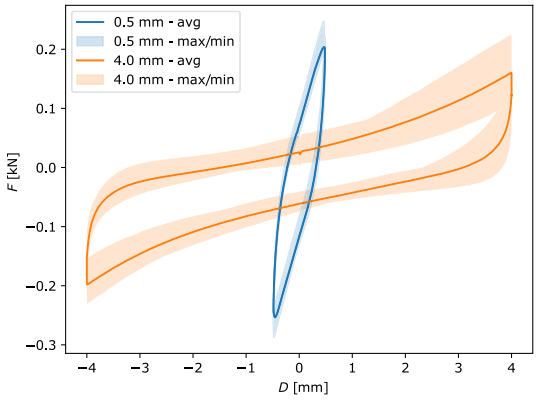

Fig. 16. Averaged hysteresis curves at the 19th cycle for the test with amplitude 0.5 mm (blue curve) and 4.0 mm (orange curve).

for the hysteresis curve with large amplitudes and low displacement amplitudes, respectively. This suggests that the mechanisms causing elastic deformation are not occurring at low shear angles only, but that a mix of elastic and permanent deformation is happening continuously.

The comparison of the hysteresis curve at the 19th cycle with the monotonic curve (cf. Fig. 17) shows that the response of the preform drastically has softened for the large amplitude cyclic test compared to the small amplitude test. The relatively small difference between the small displacement cyclic response and the monotonic response indicates that damage in the binder interface is limited, while damage is pronounced for large displacement cyclic loading and needs to be accounted for in the characterisation of the material. As discussed earlier, damage in the interface may be undesired during manufacturing as it may result in fibre wrinkling. In this case, a monotonic test is sufficient for characterising the preform material.

5. Conclusion

The purpose of the present study has been to characterise the transverse shear behaviour of a binder-stabilised preform during monotonic and cyclic loading to help with assessing preform formability in wind turbine blade manufacturing. A new test methodology was used to test the preform specimens in monotonic and cyclic shearing, with a data processing scheme developed to extract information on energy dissipated and softening of the response during cyclic deformation. For monotonic shearing, the preform specimens were loaded to a nominal shear angle of 18.0° (6 mm of displacement). The behaviour of the preform during monotonic loading was divided into two zones: in the first zone (the shear zone) the load is increasing with increasing displacement and the preform is shearing uniformly through the thickness of the specimen, while the load is dropping and the shearing is concentrated in the second zone (interface degradation zone). The monotonic loading experiments were carried out at three different deformation rates: 2 mm/min, 20 mm/min and 60 mm/min. The averaged load in the experiments increased with 11.8% when the deformation rate was increased from 2 mm/min to 20 mm/min, and with 23.4% when the rate was increased from 2 mm/min to 60 mm/min.

The preform was tested with deformation controlled cyclic loading with two different displacement amplitudes: 0.5 mm and 4.0 mm, corresponding to a nominal shear angle of 1.5° and 12.2°, respectively. The deformation rate of the cyclic tests was 20 mm/min. The results showed a reduction with a factor of 0.48 in stiffness for the tests with the large displacement amplitude at the 19th cycle, and a reduction with a factor of 0.84 for the small amplitude test.

The influence of the transverse shear properties on fibre wrinkling and defect generation is case-dependent, as it depends on the geometry of the mould used and the handling of the preform. The results generated in this paper are freely available at https://doi.org/10.17632/9m78sg3zwn.1 and may readily be used in preform modelling to help determining the formability of the preform and fibre wrinkling in the manufacturing of wind turbine blades.

CRediT authorship contribution statement

P.H. Broberg: Conceptualization, Methodology, Investigation, Formal analysis, Writing – original draft. **F. Shakibapour:** Methodology, Investigation, Writing – original draft. **J. Jakobsen:** Methodology, Writing – review & editing, Funding acquisition. **E. Lindgaard:** Conceptualization, Methodology, Writing – review & editing, Funding acquisition, Supervision. **B.L.V. Bak:** Conceptualization, Methodology, Writing – review & editing, Funding acquisition, Supervision.

Declaration of competing interest

The authors declare that they have no known competing financial interests or personal relationships that could have appeared to influence the work reported in this paper.

Data availability

The raw data required to reproduce these findings are available to download from /10.17632/9m78sg3zwn.1.

Acknowledgements

This study was completed as part of the MADEBLADES research project supported by the Energy Technology Development and Demonstration Program, Denmark, Grant no. 64019-0514.

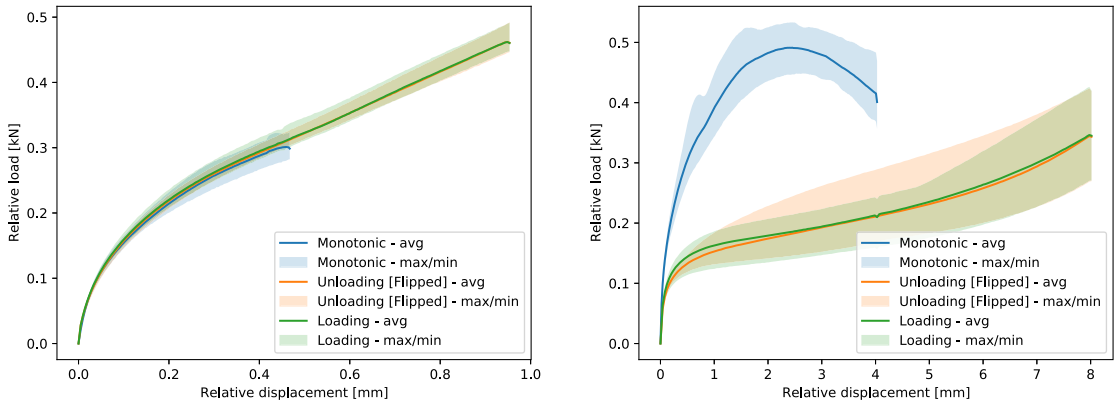

Fig. 17. Comparison of the cyclic loading, cyclic unloading and monotonic loading curve for 0.5 mm (left) and 4.0 mm (right) at the 19th cycle for a loading rate of 20 mm/min.

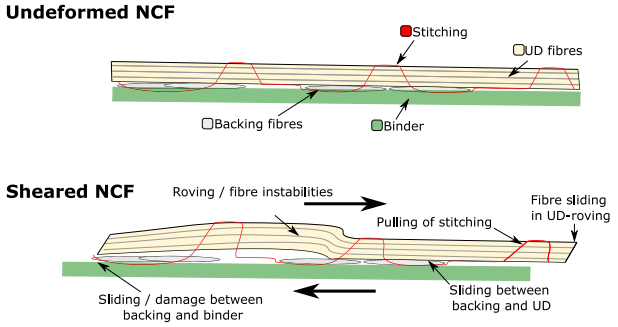

Fig. 18. Illustration of the mechanisms leading to transverse shearing of the preform.

References

[1] Farnand K, Zobeiry N, Poursartip A, Fernlund G. Micro-level mechanisms of fiber waviness and wrinkling during hot drape forming of unidirectional prepreg composites. Composites A 2017;103:168–77. http://dx.doi.org/10.1016/j.compositesa.2017.10.008.

[2] Henning F, Kärger L, Dörr D, Schirmaier FJ, Seuffert J, Bernath A. Fast processing and continuous simulation of automotive structural composite components. Compos Sci Technol 2019;171:261–79. http://dx.doi.org/10.1016/j.compscitech.2018.12.007.

[3] Schmidt S, Mahrholz T, Kühn A, Wierach P. Powder binders used for the manufacturing of wind turbine rotor blades, part 1. characterization of resin-binder interaction and preform properties. Polym Compos 2018;39(3):708–17. http://dx.doi.org/10.1002/pc.23988.

[4] Schmidt S, Mahrholz T, Kühn A, Wierach P. Powder binders used for the manufacturing of wind turbine rotor blades, Part 2. Investigation of binder effects on the mechanical performance of glass fiber reinforced polymers. J Compos Mater 2019;53(16):2261–70. http://dx.doi.org/10.1177/0021998318824784.

[5] Mesogitis TS, Skordos AA, Long AC. Uncertainty in the manufacturing of fibrous thermosetting composites: A review. Composites A 2014;57:67–75. http://dx.doi.org/10.1016/j.compositesa.2013.11.004.

[6] Azzouz R, Allaoui S, Moulart R. Composite preforming defects: a review and a classification. Int J Mater Form 2021;14(6):1259–78. http://dx.doi.org/10.1007/s12289-021-01643-7.

[7] Hsiao HM, Daniel IM. Effect of fiber waviness on stiffness and strength reduction of unidirectional composites under compressive loading. Compos Sci Technol 1996;56(5):581–93. http://dx.doi.org/10.1016/0266-3538(96)00045-0.

[8] Nelson J, Riddle T, Cairns D. Effects of defects in composite wind turbine blades – part 1: Characterization and mechanical testing. Wind Energy Sci 2017;2:641–52. http://dx.doi.org/10.5194/wes-2-641-2017.

[9] Bender J, Hallett S, Lindgaard E. Investigation of the effect of wrinkle features on wind turbine blade sub-structure strength. Compos Struct 2019;218:39–49. http://dx.doi.org/10.1016/j.compstruct.2019.03.026.

[10] Bender J, Hallett S, Lindgaard E. Parametric study of the effect of wrinkle features on the strength of a tapered wind turbine blade sub-structure. Compos Struct 2019;218:120–9. http://dx.doi.org/10.1016/j.compstruct.2019.02.065.

[11] Prodromou A, Chen J. On the relationship between shear angle and wrinkling of textile composite preforms. Composites A 1997;28(5):491–503. http://dx.doi.org/10.1016/S1359-835X(96)00150-9.

[12] Boisse P, Hamila N, Vidal-Sallé E, Dumont F. Simulation of wrinkling during textile composite reinforcement forming, Influence of tensile, in-plane shear and bending stiffnesses. Compos Sci Technol 2011;71(5):683–92. http://dx.doi.org/10.1016/j.compscitech.2011.01.011.

[13] Krogh C, Glud JA, Jakobsen J. Modeling the robotic manipulation of woven carbon fiber prepreg plies onto double curved molds: A path-dependent problem. J Compos Mater 2019;53(15):2149–64. http://dx.doi.org/10.1177/0021998318822722.

[14] Lightfoot JS, Wisnom MR, Potter K. A new mechanism for the formation of ply wrinkles due to shear between plies. Composites A 2013;49:139–47. http://dx.doi.org/10.1016/j.compositesa.2013.03.002.

[15] Allaoui S, Cellard C, Hivet G. Composites : Part A effect of inter-ply sliding on the quality of multilayer interlock dry fabric preforms. Composites A 2015;68:336–45. http://dx.doi.org/10.1016/j.compositesa.2014.10.017.

[16] Sjölander J, Hallander P, Åkermo M. Forming induced wrinkling of composite laminates: A numerical study on wrinkling mechanisms. Composites A 2016;81:41–51. http://dx.doi.org/10.1016/j.compositesa.2015.10.012.

[17] Guzman-Maldonado E, Wang P, Hamila N, Boisse P. Experimental and numerical analysis of wrinkling during forming of multi-layered textile composites. Compos Struct 2019;208:213–23. http://dx.doi.org/10.1016/j.compstruct.2018.10.018.

[18] Netzel C, Mordasini A, Schubert J, Allen T, Battley M, Hickey CM, Hubert P, Bickerton S. An experimental study of defect evolution in corners by autoclave processing of prepreg material. Composites A 2021;144(July 2020):106348. http://dx.doi.org/10.1016/j.compositesa.2021.106348.

[19] Cornelissen B, Rietman B, Akkerman R. Composites : Part A frictional behaviour of high performance fibrous tows : Friction experiments. Composites A 2013;44:95–104. http://dx.doi.org/10.1016/j.compositesa.2012.08.024.

[20] Rohatgi V, Lee LJ. Moldability of tackified fiber preforms in liquid composite molding. J Compos Mater 1997;31(7):720–44. http://dx.doi.org/10.1177/002199839703100705, arXiv:https://doi.org/10.1177/002199839703100705.

[21] Terekhov IV, Chistyakov EM. Binders used for the manufacturing of composite materials by liquid composite molding. Polymers 2022;14(1). http://dx.doi.org/10.3390/polym14010087.

[22] Broberg PH, Krogh C, Lindgaard E, Bak BLV. Simulation of wrinkling during forming of binder stabilized UD-NCF preforms in wind turbine blade manufacturing. Key Eng Mater 2022;926:1248–56. http://dx.doi.org/10.4028/p-165q46.

[23] Vanclooster K, Lomov S, Verpoest I. Simulation of multi-layered composites forming. Int J Mater Form 2010;3:695–8. http://dx.doi.org/10.1007/s12289-010-0865-2.

[24] Nosrat Nezami F, Gereke T, Cherif C. Analyses of interaction mechanisms during forming of multilayer carbon woven fabrics for composite applications. Composites A 2016;84:406–16. http://dx.doi.org/10.1016/j.compositesa.2016.02.023.

[25] Coutandin S, Wurba A-K, Luft A, Schmidt F, Dackweiler M, Fleischer J. Mechanical characterisation of the shear, bending and friction behaviour of bindered woven fabrics during the forming process. Materwiss Werksttech 2019;50:1573–87. http://dx.doi.org/10.1002/mawe.201900074.

[26] Yu F, Chen S, Harper LT, Warrior NA. Investigation into the effects of inter-ply sliding during double diaphragm forming for multi-layered biaxial non-crimp fabrics. Composites A 2021;150(August). http://dx.doi.org/10.1016/j.compositesa.2021.106611.

[27] Martin CJ, Seferis JC, Wilhelm MA. Frictional resistance of thermoset prepregs and its influence on honeycomb composite processing. Composites A 1996;27(10):943–51. http://dx.doi.org/10.1016/1359-835X(96)00037-1.

[28] Ersoy N, Potter K, Wisnom MR, Clegg MJ. An experimental method to study the frictional processes during composites manufacturing. Composites A 2005;36(11):1536–44. http://dx.doi.org/10.1016/j.compositesa.2005.02.010.

[29] Larberg YR, Åkermo M. On the interply friction of different generations of carbon/epoxy prepreg systems. Composites A 2011;42(9):1067–74. http://dx.doi.org/10.1016/j.compositesa.2011.04.010.
[30] Najjar W, Pupin C, Legrand X, Boude S, Soulat D, Santo PD. Analysis of frictional behaviour of carbon dry woven reinforcement. 2014, http://dx.doi.org/10.1177/0731684414521670.
[31] Erland S, Dodwell T, Butler R. Characterisation of inter-ply shear in uncured carbon fibre prepreg. Composites A 2015;77:210–8. http://dx.doi.org/10.1016/j.compositesa.2015.07.008.
[32] Wang L, Xu P, Peng X, Zhao K, Wei R. Characterization of inter-ply slipping behaviors in hot diaphragm preforming: Experiments and modelling. Composites A 2019;121(September 2018):28–35. http://dx.doi.org/10.1016/j.compositesa.2019.03.012.
[33] Rashidi A, Montazerian H, Yesilcimen K, Milani AS. Experimental characterization of the inter-ply shear behavior of dry and prepreg woven fabrics: Significance of mixed lubrication mode during thermoset composites processing. Composites A 2020;129(November 2019):105725. http://dx.doi.org/10.1016/j.compositesa.2019.105725.
[34] Lawrence GD, Chen S, Warrior NA, Harper LT. The influence of inter-ply friction during double-diaphragm forming of biaxial NCFs. Composites A 2023;167(August 2022):107426. http://dx.doi.org/10.1016/j.compositesa.2023.107426.
[35] Haanappel SP, Akkerman R. Shear characterisation of uni-directional fibre reinforced thermoplastic melts by means of torsion. Composites A 2014;56:8–26. http://dx.doi.org/10.1016/j.compositesa.2013.09.007.
[36] Wendling-Hivet A, Ferré MR, Allaoui S, Nunez R, Loison S, Hivet G. Study of the cohesion of carbon fiber yarns: in-plane shear behavior. Int J Mater Form 2017;10(5):671–83. http://dx.doi.org/10.1007/s12289-016-1310-y.
[37] Erland S, Dodwell TJ. Quantifying inter- and intra-ply shear in the deformation of uncured composite laminates. Adv Manuf: Polym Compos Sci 2021;7(2):25–35. http://dx.doi.org/10.1080/20550340.2021.1968190.
[38] Charmetant A, Orliac J, Vidal-Sallé E, Boisse P. Hyperelastic model for large deformation analyses of 3d interlock composite preforms. Compos Sci Technol 2012;72(12):1352–60. http://dx.doi.org/10.1016/j.compscitech.2012.05.006.
[39] Zhang Y, Sun F, Wang Y, Chen L, Pan N. Study on intra / inter-ply shear deformation of three dimensional woven preforms for composite materials. Mater Des 2013;49:151–9. http://dx.doi.org/10.1016/j.matdes.2013.02.025.
[40] Yang Z, Jiao Y, Zhu W, Xie J, Jiao W, Chen L. Experimental and numerical investigation of inter-ply shear behavior of 3D woven preform. Compos Struct 2023;304(P1):116480. http://dx.doi.org/10.1016/j.compstruct.2022.116480.
[41] ASTM C 273: Standard test method for shear properties of sandwich core materials. Standard, ASTM International; 2000.
[42] Hivet G, Allaoui S, Cam BT, Ouagne P, Soulat D. Design and potentiality of an apparatus for measuring yarn/yarn and fabric/fabric friction. Exp Mech 2012;52(8):1123–36. http://dx.doi.org/10.1007/s11340-011-9566-0.
[43] Sourki R, Crawford B, Vaziri R, Milani AS. Orientation dependency and hysteresis nature of inter-ply friction in woven fabrics. Appl Compos Mater 2021;28(1):113–27. http://dx.doi.org/10.1007/s10443-020-09846-y.
[44] Krogh C, Kepler JA, Jakobsen J. Pure and simple: investigating the in-plane shear kinematics of a quasi-unidirectional glass fiber non-crimp fabric using the bias-extension test. Int J Mater Form 2021;14(6):1483–95. http://dx.doi.org/10.1007/s12289-021-01642-8.